

1 **Temporal variations in sea ice resistivity: resolving anisotropic microstructure through**
2 **cross-borehole dc resistivity tomography**

3

4 K.A. Jones¹, M. Ingham¹, D.J. Pringle^{2,3} and H. Eicken²

5

6 ¹School of Chemical & Physical Sciences, Victoria University of Wellington, PO Box 600,
7 Wellington, New Zealand

8 ²Geophysical Institute, University of Alaska, Fairbanks, Alaska, USA

9 ³Arctic Region Supercomputing Centre, University of Alaska, Fairbanks, Alaska, USA

10

11

12

13 **Abstract**

14

15 The distribution and connectivity of brine pockets in first-year sea ice has a determining
16 influence on the bulk properties of the ice and its interaction with the environment. The
17 structure of the brine network depends upon both temperature and salinity, and a full
18 understanding of the temporal evolution of sea ice physical properties requires measurements
19 that are sensitive to the microstructure, and can also be made without disturbing the natural
20 state of the ice. Direct current resistivity techniques are suited to this as the brine fraction is
21 orders of magnitude more conductive than solid ice. However, due to the preferential vertical
22 alignment of brine inclusions, the bulk resistivity of first-year sea ice is anisotropic. Although
23 this makes the interpretation of surface resistivity soundings extremely difficult,
24 consideration of the theory of resistivity measurements in an anisotropic medium shows that
25 the anisotropic resistivity structure may be resolved through cross-borehole measurements.
26 Borehole pairs with one current and one potential electrode in each hole allow the
27 determination of the horizontal component of the anisotropic bulk resistivity (ρ_H). Use of four
28 boreholes allows an estimate of the geometric mean resistivity (ρ_m) to be derived. Combining
29 these measurements allows calculation of the vertical resistivity (ρ_V). This is illustrated by
30 measurements made in first-year sea ice near Barrow, Alaska in April – June 2008. Over this
31 period significant changes in resistivity are observed which may be shown to be related to
32 both the brine volume fraction and the microstructure of the ice.

33

34

35 **1. Introduction**

36

37 Sea ice covers a large area of high latitude ocean in the Arctic and Antarctic regions. While
38 sea ice extent varies seasonally, at maximum approximately 7% of the Earth's surface is
39 covered, making sea ice one of the largest biomes on Earth. Not only does sea ice regulate the
40 exchange of heat between the ocean and the atmosphere, but its permeability to fluids
41 controls brine exchange with the ocean, and its physical strength allows it to provide a
42 surface for ice based activities. Despite the importance of sea ice, a detailed understanding
43 and representation of many of its physical properties is still lacking. This is needed to give
44 greater accuracy to both climate models and global circulation models (Dieckmann and
45 Hellmer, 2003). In this paper we present a significant advance towards a better understanding
46 of the physical properties of sea ice and their seasonal evolution with temperature, salinity
47 and brine volume fraction.

48

49 During the formation of sea ice, brine becomes trapped in pockets within the solid ice matrix.
50 These range in size from sub-millimeter pores to large connected networks of channels
51 several millimeters in diameter and extending over several decimeters. The connectivity of
52 the brine pockets is highly sensitive to variations in temperature and bulk ice salinity, and
53 strongly affects physical, optical, (Eicken, 2003) and biological properties (Krembs et al.,
54 2000) of sea ice. It is through these properties that sea ice has an influence on the global
55 climate (Comiso, 2003) and ecosystems. An understanding of the manner in which the
56 internal microstructure of sea ice changes in response to changes in temperature and salinity
57 is therefore crucial for a fuller understanding of the role that sea ice plays in a range of
58 contexts. The existence and connectivity of brine channels in the ice affects the transport of
59 heat through the ice (Perovich, 1998; Weeks, 1998). By estimating the latent heat release
60 associated with convective overturning and refreezing of brine, Pringle et al. (2007) have
61 estimated that internal brine motion within the ice may somewhat enhance the overall heat

62 flux. Brine inclusions also control the manner in which the ice interacts with electromagnetic
63 radiation (Hallikainen & Winebrenner, 1992; Cherkaeva & Golden, 1998), while fluid
64 permeability is important for nutrient transport through the ice (Fritsen et al., 1994).
65 Theoretical calculations of the physical properties of sea ice have generally been based on
66 effective medium theories (e.g. Tinga et al., 1973) and, more recently, on percolation theory
67 (Golden et al., 1998, 2007). Nevertheless, despite the relevance of the microstructure of sea
68 ice to determining its role in the global climate system, there are few field measurements of
69 the temporal variation in the physical properties of sea ice with which such theoretical
70 calculations can be compared.

71

72 The internal structure of sea ice ought to be able to be studied using any transport property to
73 which the brine and ice components contribute differently. The microstructure, thermal
74 evolution, fluid transport and permeability of sea ice brine inclusions have been studied by
75 several authors using NMR techniques (Callaghan et al., 1998, 1999; Eicken et al., 2000;
76 Mercier et al., 2005), bail-test and fluorescent tracer methods (Freitag and Eicken, 2003), x-
77 ray computed tomography (Kawamura, 1988, Pringle et al., 2009b), and impedance
78 measurements (Notz and Worster, 2008; Pringle et al., 2009a). However, in practice there are
79 severe difficulties in making accurate measurements as most such methods inevitably disturb
80 the ice from its natural state, such as brine loss from samples that need to be extracted for
81 measurements in the laboratory or artificial brine motion induced by insertion of large probes.

82

83 In this context, measurements of electrical resistivity hold some promise, since the large
84 resistivity contrast between brine and solid ice opens a path towards indirect probing of other
85 key ice properties. Furthermore, direct current (dc) geoelectric soundings, widely used in
86 shallow geophysical studies, are generally made using surface electrodes and do not therefore

87 disturb the natural structure of the sub-surface. However, due to the preferential vertical
88 alignment of brine inclusions, the bulk resistivity of sea ice is anisotropic and, as a result,
89 surface resistivity soundings can be shown (e.g. Bhattacharya and Patra, 1968) to be sensitive
90 to only the geometric mean resistivity of the anisotropic medium. This has been clearly noted
91 in previous resistivity measurements made on sea ice (e.g. Fujino and Suzuki, 1963; Thyssen
92 et al., 1974; Timco, 1979; Buckley et al., 1986, Ingham et al., 2008) which have also shown
93 that surface soundings underestimate the true thickness of the anisotropic sea ice cover. This
94 makes the interpretation of soundings in terms of variation of geometric mean resistivity with
95 depth problematic.

96

97 Recently Ingham et al. (2008) have demonstrated that an alternative dc resistivity technique,
98 that of cross-borehole tomography, can be used to measure the horizontal component of the
99 anisotropic resistivity structure of sea ice. This technique involves making resistivity
100 measurements using vertical strings of electrodes frozen into the ice while it is relatively thin
101 and that are subsequently embedded into the growing ice sheet. Although insertion of
102 electrode strings, and their subsequent freezing in, disturbs the ice structure immediately
103 adjacent to the boreholes, the bulk of ice between the electrode strings is undisturbed and it is
104 through this that current passes. Such measurements therefore largely sample ice in its natural
105 state. Ingham et al. (2008) reported trial measurements made at Barrow, Alaska that clearly
106 suggested that changes in the horizontal component of resistivity of the ice occurred over the
107 period of spring warming.

108

109 In this paper we discuss, and present results from, a further development of the use of
110 resistivity techniques to study the physical properties of sea ice. We start by readdressing,
111 from the point of view of the theory of resistivity measurements in an anisotropic medium,

the ability or inability of cross-borehole techniques to measure not only the horizontal component of the anisotropic resistivity, but also the vertical component and the geometric mean resistivity. Following consideration of an infinite anisotropic medium (section 2) we consider an anisotropic medium bounded by air above and by a highly conducting half-space, representative of sea water, below (section 3). We demonstrate how in this situation, in addition to resolving the horizontal component of resistivity, cross-borehole measurements supported by the results of model calculations can yield the geometric mean resistivity and its variation with depth in the ice. This consequently allows the derivation of the vertical component of the resistivity, thus determining the complete resistivity structure. We illustrate this both with inversions of synthetic data generated from forward numerical calculations, and by presenting results from the actual application to real sea ice (section 4). These results, from a series of 6 sets of measurements made near Barrow Alaska over the period of spring warming, clearly show a temporal evolution in the electrical properties of sea ice. They indicate that the resistivity technique holds much promise as a vehicle for developing a greater understanding of the temporal variation of the microstructure of sea ice and the impact of this on the physical properties of sea ice that are crucial to its role in the climate system.

2. Electrical resistivity measurements in an infinite uniform anisotropic medium

In first-year sea ice formed under quiescent conditions the preferential vertical alignment of the brine inclusions means that the bulk resistivity structure of the ice is anisotropic, with the vertical component of the bulk resistivity lower than the horizontal component. Although it is possible that in the presence of steady ocean currents the horizontal resistivity itself may exhibit some anisotropy, particularly in the case of landfast sea ice (Kovacs and Morey,

1978), in the present analysis we treat this as typically insignificant compared to the anisotropy between the vertical and horizontal resistivity.

Following Bhattacharya & Patra (1968), as detailed in the Appendix of Ingham et al. (2008), in an infinite uniform anisotropic medium in which the principal resistivities (ρ_H , ρ_V) are horizontal and vertical the potential at a location (x_j, y_j, z_j) due to a current I injected into the medium from a single electrode at (x_i, y_i, z_i), is given by

$$V = \frac{I\rho_m}{4\pi r_{ij} \left\{ 1 + (\lambda^2 - 1) \frac{(z_i - z_j)^2}{r_{ij}^2} \right\}^{1/2}} \quad (1)$$

where ρ_m is the geometric mean resistivity

$$\rho_m = \sqrt{\rho_H \rho_V} \quad (2)$$

λ is an anisotropy coefficient defined as

$$\lambda = \sqrt{\frac{\rho_V}{\rho_H}} \quad (3)$$

and

$$r_{ij} = \sqrt{(x_i - x_j)^2 + (y_i - y_j)^2 + (z_i - z_j)^2}.$$

Equation (1) may be expressed in the simpler form

$$V = \frac{I\rho_m}{4\pi \{X_{ij}^2 + \lambda^2 (z_i - z_j)^2\}^{1/2}} \quad (4)$$

where

$$X_{ij} = \sqrt{(x_i - x_j)^2 + (y_i - y_j)^2} \quad (5)$$

is the horizontal separation between the current and potential electrodes.

The majority of electrical imaging surveys make use of four electrodes. Two electrodes are used to introduce current into the medium, one being a current source the other a sink. The potential difference is then measured between the remaining two electrodes. For a four electrode system in which current is injected into an anisotropic medium through an electrode C_1 at (x_1, y_1, z_1) , is taken out of the medium through an electrode C_2 at (x_2, y_2, z_2) , and in which the potential difference ΔV is measured between electrodes P_1 and P_2 at (x_3, y_3, z_3) and (x_4, y_4, z_4) respectively, equation (1) may be used to show that

$$\Delta V = \frac{I}{4\pi} \rho_m (T_{13} - T_{14} - T_{23} + T_{24}) \quad (6)$$

where

$$T_{ij} = \frac{1}{r_{ij} \left\{ 1 + (\lambda^2 - 1) \frac{(z_i - z_j)^2}{r_{ij}^2} \right\}^{1/2}}$$

Starting from (6) it is possible to investigate which, if any, combinations of electrodes embedded in an infinite uniform anisotropic medium will allow the direct measurement of individual components of the anisotropic resistivity. This is done by considering the fact that if measurements were made in a medium of uniform isotropic resistivity ρ then the equivalent form of equation (6) would be

$$\Delta V = \frac{I}{4\pi} \rho \left\{ \frac{1}{r_{13}} - \frac{1}{r_{14}} - \frac{1}{r_{23}} + \frac{1}{r_{24}} \right\} \quad (7)$$

Determining the conditions under which (6) reduces to (7) when ρ is considered to be ρ_m , ρ_V or ρ_H , shows which electrode combinations, if any, it is possible to use to yield a determination of the relevant resistivity.

Although our interest is primarily in the microstructure of sea ice, for which $\lambda < 1$, the development that follows can easily be adapted for cases where $\lambda > 1$.

2.1. Measurement of ρ_H

The measurement of the horizontal component of the anisotropic resistivity has previously been discussed by Ingham et al. (2008). We summarise those arguments here. As outlined above measurements can be interpreted in terms of the horizontal component if equation (6), rewritten using (2) and (3) as

$$\Delta V = \frac{I}{4\pi} \rho_H \lambda (T_{13} - T_{14} - T_{23} + T_{24}) \quad (8)$$

is identical to the following form of equation (7)

$$\Delta V = \frac{I}{4\pi} \rho_H \left\{ \frac{1}{r_{13}} - \frac{1}{r_{14}} - \frac{1}{r_{23}} + \frac{1}{r_{24}} \right\} \quad (9)$$

This will be true if in each of the T_{ij} terms in (8)

$$1 + (\lambda^2 - 1) \frac{(z_i - z_j)^2}{r_{ij}^2} = \lambda^2 \quad (10)$$

This is satisfied if

$$(z_i - z_j)^2 = r_{ij}^2$$

which implies that either

$$(x_i - x_j)^2 + (y_i - y_j)^2 = 0 \quad (11a)$$

or, alternatively, that

$$|z_i - z_j| \gg \sqrt{(x_i - x_j)^2 + (y_i - y_j)^2} \quad (11b)$$

200

201 Condition (11b) is met when the current and potential electrodes are much more widely
202 separated vertically than they are horizontally. Although the present discussion concerns an
203 anisotropic medium of infinite extent it is clear that this condition will have practical
204 limitations in a real situation in which the anisotropic structure under study is relatively thin.
205 As this is the case for first-year sea ice, for which typical thicknesses are < 2 m, we do not
206 consider this possibility.

207

208 Condition (11a) corresponds to the current electrode and the potential electrode having the
209 same horizontal location i.e. being in the same borehole. Applying the same condition to all
210 four T_{ij} terms in equation (8) requires all four electrodes to be in a single borehole. Timco
211 (1979) effectively met this condition by using four electrodes aligned vertically in the side of
212 an ice pit to measure ρ_H . However, in the case of four electrodes within the same borehole the
213 formation of an anomalous halo around the electrode string when it is frozen into the ice
214 raises the likelihood that measurements will be significantly affected by ice that is not in its
215 natural state. We therefore exclude this option also.

216

217 An additional possibility, as described by Ingham et al. (2008), is to consider the situation
218 where C_1 and P_1 have the same horizontal location (i.e. $x_1 = x_3, y_1 = y_3$), as do C_2 and P_2 ($x_2 =$
219 $x_4, y_2 = y_4$). In a practical situation this is equivalent to using 2 boreholes, each containing one
220 current and one potential electrode. This simplifies the expressions for T_{13} , and T_{24} to

221
$$\lambda T_{ij} = \frac{1}{|z_i - z_j|}$$

222 while those for T_{14} and T_{23} become

$$\lambda T_{ij} = \frac{\lambda}{\left\{ (X_1 - X_2)^2 + (z_i - z_j)^2 \right\}^{1/2} \left\{ 1 + (\lambda^2 - 1) \frac{(z_i - z_j)^2}{(X_1 - X_2)^2 + (z_i - z_j)^2} \right\}^{1/2}}$$

where $X_1 - X_2$ is the horizontal distance between the boreholes.

The expressions for λT_{13} and λT_{24} are clearly equal to the first and last terms on the right hand side of (9). Consider the case that $\lambda < 1$ and the separation of the boreholes is 10 times the smallest vertical electrode separation i.e.

$$|z_i - z_j| = n \cdot 0.1 |X_1 - X_2| \quad (12)$$

where n is an integer. Ingham et al. (2008) demonstrate that in these circumstances the dependency on λ in the expressions for λT_{14} and λT_{23} may be approximated as

$$\frac{\lambda}{\left\{ 1 + (\lambda^2 - 1) \frac{(z_i - z_j)^2}{(X_1 - X_2)^2 + (z_i - z_j)^2} \right\}^{1/2}} \approx \frac{\lambda}{\left\{ 1 + (\lambda^2 - 1) \frac{0.01n^2}{1 + 0.01n^2} \right\}^{1/2}} \sim \lambda$$

For $|X_1 - X_2| = 1$, the ratios of the terms in T_{14} and T_{23} to those in T_{13} and T_{24} are then given by

$$(\lambda T_{14}, \lambda T_{23}) : (\lambda T_{13}, \lambda T_{24}) \sim \frac{n\lambda}{10} \quad (13)$$

If current and potential electrode pairs are chosen such that $n \leq 2$ then, for reasonable values of anisotropy (i.e. λ less than about 0.6, consistent with values reported by Thyssen et al., 1974 and Buckley et al., 1986), terms in T_{14} and T_{23} may be ignored compared to those in T_{13} and T_{24} .

241 It also follows that for $|X_1 - X_2| = 1$, $\lambda < 1$, and values of $n \leq 2$ the terms in (9) in $\frac{1}{r_{14}}$ and
 242 $\frac{1}{r_{23}}$ will be significantly less than 1/5 of the size of the terms in $\frac{1}{r_{13}}$ and $\frac{1}{r_{24}}$. Ignoring these
 243 smaller terms in equation (9) gives an error of $\sim 10\%$ in the spatial term and within this error
 244 equations (8) and (9) may both be approximated by

$$245 \quad \Delta V = \frac{I}{4\pi} \rho_H \left\{ \frac{1}{|z_1 - z_3|} + \frac{1}{|z_2 - z_4|} \right\} \quad (14)$$

246
 247 Thus the use of electrodes at two horizontal locations under the conditions that (i) $\lambda < 1$; and
 248 (ii) the electrodes are positioned such that equation (12) holds, with n small; allows
 249 measurements to be made which are sensitive to ρ_H .

250

251 **2.2. Measurement of ρ_m**

252

253 To provide a measure of the geometric mean resistivity ρ_m , equation (6) must be equivalent to
 254 the expression

$$255 \quad \Delta V = \frac{I}{4\pi} \rho_m \left\{ \frac{1}{r_{13}} - \frac{1}{r_{14}} - \frac{1}{r_{23}} + \frac{1}{r_{24}} \right\}$$

256 This requires conditions on the denominators of the expressions for the T_{ij} of the form

$$257 \quad 1 + (\lambda^2 - 1) \frac{(z_i - z_j)^2}{r_{ij}^2} = 1 \quad (15)$$

258 Equation (15) may be satisfied if

$$259 \quad z_i = z_j$$

260 Extending this so that the conditions are imposed upon all four T_{ij} terms implies that all four
 261 electrodes must be at the same vertical level

$$z_1 = z_2 = z_3 = z_4$$

263

264 As it is undesirable to use the same electrode for both current injection and potential
 265 measurement, in order to make measurements that will determine ρ_m it is therefore necessary
 266 to use a minimum of 4 electrodes at separate horizontal locations (i.e. a minimum of 4
 267 boreholes). In the most general situation where ρ_m is $\rho_m(x, y, z)$, for n boreholes, discounting
 268 measurements which simply reverse either the current or potential electrodes, there are
 269 therefore $n!/4$ independent measurements that may be made for each vertical level at which
 270 there is an electrode.

271

272 Measurements of ρ_m may also be obtained by removing either or both of one current and one
 273 potential electrode to infinity. For example, under the circumstance of C_2 being at infinity,
 274 the expressions for both T_{23} and T_{24} are zero and as long as $z_1 = z_3 = z_4$ then T_{13} and T_{14} are
 275 $1/r_{13}$ and $1/r_{14}$ respectively, and both equations (6) and (7) reduce to

$$\Delta V = \frac{I}{4\pi} \rho_m \left\{ \frac{1}{r_{13}} - \frac{1}{r_{14}} \right\}$$

277 Similarly, if P_2 is at infinity and $z_1 = z_2 = z_3$ (6) and (7) reduce to

$$\Delta V = \frac{I}{4\pi} \rho_m \left\{ \frac{1}{r_{13}} - \frac{1}{r_{23}} \right\}$$

279

280 Clearly therefore, using 4 or more electrodes all at separate horizontal locations, there are
 281 electrode combinations that may be used to measure the geometric mean resistivity of an
 282 infinite uniform anisotropic medium.

283

284

2.3. Measurement of ρ_V

To ascertain which, if any, electrode combinations may be used to make measurements which can be used to derive the vertical component of the resistivity ρ_V it is necessary to use equations (2) and (3) to recast equation (6) in the form

$$\Delta V = \frac{I}{4\pi} \frac{\rho_V}{\lambda} (T_{13} - T_{14} - T_{23} + T_{24})$$

For this equation to take the form which would indicate that measurements are responsive to ρ_V , namely

$$\Delta V = \frac{I}{4\pi} \rho_V \left\{ \frac{1}{r_{13}} - \frac{1}{r_{14}} - \frac{1}{r_{23}} + \frac{1}{r_{24}} \right\}$$

requires that expressions of the form

$$\frac{1}{1 + (\lambda^2 - 1) \frac{(z_i - z_j)^2}{r_{ij}^2}} = \lambda^2 \quad (16)$$

are satisfied. Equation (16) reduces to

$$\frac{(z_i - z_j)^2}{r_{ij}^2} = -\frac{1}{\lambda^2} \quad (17)$$

which clearly does not have a real solution. It may therefore be concluded that there are no possible electrode combinations that may be interpreted in terms of the vertical component of the anisotropic resistivity.

Having looked at the idealised case of an infinite uniform anisotropic medium, we now turn our attention to a better representation of sea ice - the case of a bounded medium.

3. Cross-borehole measurements in a bounded anisotropic medium

306

307 In reality cross-borehole resistivity tomography seeks to image the relatively near-surface
308 structure in a half-space of variable resistivity. Although the above theory suggests that
309 measurement of the horizontal component and geometric mean resistivity are possible in an
310 infinite anisotropic medium, this will not necessarily be the case in a bounded anisotropic
311 medium. It is necessary therefore to see how the above results are modified by the inclusion
312 of boundaries.

313

314 To consider the effect of boundaries on the potential at a given point in the medium due to a
315 current source elsewhere in the medium we make use of an analogy made in many applied
316 geophysics texts (e.g. Telford et al., 1977) between current flow through a boundary between
317 two media and the optical case of a point light source in one medium separated from another
318 medium by a semi-transparent mirror with reflection coefficient k_1 . In the optical case the
319 light intensity at a point in the first medium is a combination of the intensity due to the point
320 source and the intensity due to its image in the mirror, diminished by the reflection
321 coefficient. Similarly, the electric potential at a point in the same medium as a point current
322 source can be considered as the sum of the potential due to the source and a generally
323 diminished potential due to an image source. The intensity or potential at a point in the
324 second medium is due only to the point source, but diminished by the transmission
325 coefficient of the boundary.

326

327 This situation is illustrated in Fig. 1 in which two semi-infinite media are separated by a
328 boundary at $z = 0$ with a reflection coefficient k_1 . Current is injected and potential measured
329 in the lower medium which is assumed to be anisotropic. The potential at electrode P at $(x_j,$

330 z_j) due to current I injected at electrode C at (x_i, z_i) may be expressed, using the form of
 331 equations (4) and (5), as

$$332 \quad V = \frac{I\rho_m}{4\pi\{X_{ij}^2 + \lambda^2(z_i - z_j)^2\}^{1/2}} + \frac{k_1 I\rho_m}{4\pi\{X_{ij}^2 + \lambda^2(z_i + z_j)^2\}^{1/2}} \quad (18)$$

333

334 In (18) the first term is the potential due to the actual electrode through which current is
 335 injected. The second term is the potential due to the image of C in the boundary. k_1 is the
 336 reflection coefficient in the boundary. For current from a source in a medium of resistivity ρ_1 ,
 337 incident on a boundary with a medium of resistivity ρ_2 , the reflection coefficient is defined as
 338 $k = (\rho_2 - \rho_1)/(\rho_2 + \rho_1)$, thus for the practical case of the upper medium being air ($\rho_2 \sim \infty$), $k_1 =$
 339 1.

340

341 The addition of a second boundary at depth t with reflection coefficient k_2 modifies (18)
 342 further. In this situation the anisotropic medium is confined to the region $0 \leq z \leq t$ and
 343 multiple images of the current source occur in both boundaries. As given for example by
 344 Keller & Frischknecht (1966), the potential observed at an electrode (P) in the anisotropic
 345 medium at (x_j, y_j, z_j) due to current injected into that medium by an electrode (C) at (x_i, y_i, z_i)
 346 is given by

347

$$348 \quad V_{ij} = \frac{I\rho_m}{4\pi} \left\{ \frac{1}{\{X_{ij}^2 + \lambda^2[z_i - z_j]^2\}^{1/2}} + \sum_{n=1}^{\infty} \frac{k_2^{n-1}}{\{X_{ij}^2 + \lambda^2[z_i + z_j + 2(n-1)t]^2\}^{1/2}} \right.$$

$$349 \quad \left. + \sum_{n=1}^{\infty} \frac{k_2^n}{\{X_{ij}^2 + \lambda^2[z_i - z_j - 2nt]^2\}^{1/2}} + \sum_{n=1}^{\infty} \frac{k_2^n}{\{X_{ij}^2 + \lambda^2[z_i + z_j - 2nt]^2\}^{1/2}} \right.$$

$$350 \quad \left. + \sum_{n=1}^{\infty} \frac{k_2^n}{\{X_{ij}^2 + \lambda^2[z_i - z_j + 2nt]^2\}^{1/2}} \right\} \quad (19)$$

in which it is been assumed that $k_1 = 1$. Assuming that $\rho_m \approx 10 - 100 \text{ } \Omega\text{m}$ and that the underlying sea-water has $\rho_{sw} \approx 0.4 \text{ } \Omega\text{m}$, k_2 will be in the range of -0.92 to -0.99 (the value being negative as ρ_{sw} is less than ρ_m). The first term in (19) represents the potential due to the "direct path" within the anisotropic medium from C to P , whereas the four summations arise from considering the multiple "reflections" from the two boundaries. Similar expressions involving both "direct path" terms and infinite series arising from reflections can be deduced for the other possible combinations of locations of current and potential electrodes: (i) C in the anisotropic medium, P in the underlying half-space; (ii) C in the underlying half-space, P in the anisotropic medium; and (iii) both C and P in the underlying half-space.

3.1. Measurement of ρ_H

The effect on the measurement of ρ_H of the anisotropic medium being confined to the depth range $0 \leq z \leq t$, and there being a highly conducting half-space beneath, can be assessed by considering how potential differences calculated from expressions such as (19) compare to those that would exist in an infinite anisotropic medium. As before, the potential difference measured between electrodes in two boreholes separated by horizontal distance X_{ij} is dominated by the potential terms arising from current and potential electrodes that are in the same borehole ($X_{ij} = 0$). As above, we also consider $z_j = z_i + 0.1 \text{ m}$. Numerical calculation shows that for the relevant likely values of k_2 the four infinite series converge after a few hundred terms. The k_2 dependence in each of the four summations means that whereas the first summation (S_1) is positive, the other three (S_2 to S_4) are negative. For a typical thickness of sea ice of $t = 1.4 \text{ m}$, and $z_i = 0.1 \text{ m}$ (i.e. electrodes close to the upper surface of the ice) $\Sigma S_i = S_1 + S_2 + S_3 + S_4$ is positive and, approximately independently of the value of λ , about 20%

of the size of the primary or "direct path" term in (19). The value of ΣS_i decreases with increasing z_i , being ~ 0 at $z_i = 0.4$ m, and negative and about 66% of the magnitude of the primary potential at $z_i = 1.2$ m, 0.2 m above the ice-water interface. Thus, even in a bounded anisotropic medium with the typical thickness and parameters relevant to sea ice it appears that estimates of the horizontal component of the resistivity are likely to be within a factor of about 2 of the true value.

To test this a synthetic dataset has been generated from the appropriate expressions such as (19) for the case of $\rho_m = 100 \text{ } \Omega\text{m}$ and $\lambda = 0.1$ (i.e. $\rho_H = 1000 \text{ } \Omega\text{m}$). The synthetic dataset comprised over 2000 separate electrode combinations satisfying the restrictions discussed above that allow a measurement of ρ_H to be made. The synthetic data were inverted using the code Res3dinvTM produced by Geotomo Software to derive 3D models of the horizontal resistivity structure in the volume contained between the boreholes. The code uses a smoothness constrained least-squares inversion (deGroot-Hedlin & Constable, 1990; Sasaki, 1992). Although the code allows for matrix solution using a quasi-Newton optimisation technique (Loke & Barker, 1996), all inversions were carried out using a conventional Gauss-Newton method (Loke & Dahlin, 2002) which is more appropriate in situations in which large resistivity contrasts, such as between sea ice and underlying sea water, exist. The result of the 3D inversion of the synthetic data is presented in Fig. 2 which shows the mean value of resistivity in each 0.1 m thick layer of the derived 3D resistivity structure.

It is clear from these results that, given the approximations in the theoretical development, ρ_H is indeed recovered with a good degree of accuracy at all depths within the anisotropic layer between the surface and 1.3 m depth. Only in the layer (1.3 - 1.4 m), i.e. immediately above the lower interface, is the true horizontal resistivity significantly underestimated. The low

resistivity of the underlying sea water (set at $0.4 \Omega\text{m}$ for the generation of the synthetic data) is also faithfully recovered. It should be noted that in a real situation the thickness of the anisotropic layer of sea ice is generally known from other measurements. As a result the resistivity below this depth can be constrained to the known resistivity of sea water, as has been applied in the 3D inversion the result of which shown in Fig. 2.

3.2. Measurement of ρ_m

For measurement of ρ_m , using four electrodes at the same level on the corners of a $1 \text{ m} \times 1 \text{ m}$ square, the situation is very different. In this case, as $X_{ij} = 1 \text{ m}$ or $\sqrt{2} \text{ m}$, not only is the "direct path" term in (19) significantly smaller, but, for typical thicknesses $t \sim 1\text{-}2 \text{ m}$, all the S_i are of similar magnitude and $\Sigma S_i < 0$. This results not only in the individual potentials due to current being injected or removed from the medium being reduced, but also in the potential difference between P_1 and P_2 being underestimated compared to the case of the infinite anisotropic medium, significantly so for small values of λ . The degree of underestimation depends also on the thickness, t , the depth within the ice of the electrodes being used, and, as k_2 depends upon the resistivity contrast between ρ_m and the underlying sea-water, also on the actual value of ρ_m . However, given the likely restricted range of values of k_2 this latter dependence is weak.

The underestimation ρ_m is illustrated in Fig. 3 which shows the results of 3D inversions of synthetic data sets for different values of anisotropy λ for a thickness $t = 1.4 \text{ m}$ and a true value of geometric mean resistivity $\rho_m = 100 \Omega\text{m}$. The electrode combinations used in generating the synthetic data correspond to those applicable for the measurement of ρ_m in an

infinite anisotropic medium. Shown in Fig. 3, for different values of λ , are the average values of resistivity in each layer of the derived 3D resistivity structure. The spatial grid used in the inversion means that in each case these represent an average over 400 cells in each layer. Even for $\lambda = 0.5$, in the upper 1 m of the anisotropic region, the recovered value of ρ_m is only about 70% of the true value. Closer to the ice-water interface the recovered value drops to about 40% of the true value. Similar, but increasingly severe underestimation of ρ_m occurs for decreasing values of λ down to about 0.2. For yet smaller values of λ the recovered value of ρ_m is of the order of only 1% of the true value and has a more complicated variation with depth.

Clearly, once a bounded anisotropic medium of typical thickness is considered, obtaining reliable measurements of geometric mean resistivity of sea ice through dc cross-borehole tomography is not necessarily straightforward. Nevertheless the generation of synthetic data sets from expressions of the form of (19) using the initial criteria for measurement of ρ_m does present a potential resolution of this problem. Inversion of such synthetic data to recover model resistivity values (hereafter referred to as ρ_m^M), makes it possible to derive an empirical parameterization of the relationship between the true value of ρ_m and the recovered value ρ_m^M for different values of t and λ . As t is generally known through independent measurement, and a good estimate of the horizontal component of the resistivity ρ_H can be recovered from cross-borehole measurements, as discussed above, this might allow both ρ_m and λ to be determined as described below.

For example, for a given thickness t of ice the average value of resistivity at some depth, recovered from a 3D inversion of synthetic data generated for a measurement of ρ_m may be expressed as

$$\rho_m^M = F_z(\lambda)\rho_m \quad (20)$$

where $F_z(\lambda)$ is a polynomial in the anisotropy coefficient. The form of the polynomial, which describes how the derived value of resistivity, ρ_m^M , is related to the true geometric mean resistivity, ρ_m , can be determined from inversion of synthetic data sets generated for different values of λ , such as those shown in Fig. 3. Using (2) and (3) equation (20) may be expressed as

$$\rho_m^M = \lambda F_z(\lambda)\rho_H \quad (21)$$

In principal for any given situation, not only can the form of $F_z(\lambda)$ be deduced from inversion of synthetic data for the particular ice thickness, but ρ_m^M and ρ_H as functions of depth can be determined from inversion of real data. This then allows a value for λ to be found from numerical solution of (21) for each depth range in the resulting 3D models, and an estimate of the actual value of ρ_m as a function of depth can then be determined from (20).

As an example, in the depth range 0.5-0.6 m in ice of thickness 1.4 m, the results presented in Fig. 3 suggest that for $\lambda \leq 0.5$ the function $F_z(\lambda)$ can be represented to a high degree of accuracy by a fourth order polynomial

$$F_z(\lambda) = -57.411\lambda^4 + 47.077\lambda^3 - 7.1312\lambda^2 + 0.3452\lambda \quad (22)$$

For the specific case of $\lambda = 0.1$, the inversion of the synthetic data yields a value of ρ_m^M in this depth range of 0.748 Ωm . Additionally, the results in Fig. 2 show that the inversion of the separate synthetic dataset to determine ρ_H for the case $\rho_m = 100 \Omega\text{m}$, $\lambda = 0.1$ in this depth

range gives a recovered value of ρ_H of 1105 Ωm . Thus (21) allows λ to be found as the numerical solution to

$$0.748 = (-57.411\lambda^5 + 47.077\lambda^4 - 7.1312\lambda^3 + 0.3452\lambda^2)1105$$

The result is a value of $\lambda = 0.111$, very close to the true value of 0.1 used in the generation of the synthetic datasets.

Although the above procedure appears, at first sight, to be a resolution of the problem of determining ρ_m , there remain a number of complicating factors when applying this to a real situation. These include (1) the structure of real sea ice may well include a variation in λ with depth which is not incorporated into the synthetic models; (2) in real sea ice the ice-water interface, modelled as a sharp boundary, is not sharply defined; (3) the reliance on the results of 3D inversions, both of real and synthetic data, may well introduce problems of resolution of resistivity structure; and (4) even in the inversions of synthetic data it is clear, for example from Fig. 3, that the derived values of ρ_m^M are relatively insensitive to λ for values of $\lambda \leq 0.1$. Quantifying the uncertainty in derived values of ρ_m resulting from these factors is non-trivial, but as a consequence it is likely that interpretation of values of ρ_m derived in the manner described above should bear in mind that these may only be correct to within a factor of the order of perhaps 3-4.

Given the degree of uncertainty introduced by the above factors it is worth considering the magnitude of resistivity changes that are likely to occur as the internal microstructure of sea ice changes due to expansion and connection of brine pockets and channels within the ice. A simple means of doing this is to consider the Hashin-Shtrikman limits (Hashin & Shtrikman, 1962) for the resistivity of a 2-phase mixture in which isolated spheres of conductivity σ_2 are

surrounded by a connected matrix of conductivity σ_1 . The lower and upper limits of bulk resistivity of the mixture (occurring respectively when σ_1 or σ_2 represents the better conductor) are shown in Fig. 4 for the case of a mixture of materials with conductivities (resistivities) of 2.5 S/m (0.4 Ω m) and 0.00167 S/m (600 Ω m). As can be seen, for any volume fraction of high conductivity component above about 0.5%, the decrease in bulk resistivity between the situations of isolated high conductivity spheres (i.e. brine pores) and a connected network of high conductivity is 1-3 orders of magnitude. It is clear therefore that, in terms of tracking the changes that occur in the bulk resistivity of sea ice as brine pores expand and connect, the ability to resolve between, for example, bulk resistivities of even 200 and 600 Ω m is not critical. In contrast the ability to distinguish bulk resistivities of 20 and 200 Ω m should enable the development of interconnected brine pore networks to be detected.

4. Field measurements on first-year landfast sea ice

To demonstrate the application of cross-borehole measurements to recovering the anisotropic resistivity structure in a real situation we present results from a sequence of six separate sets of measurements made on first-year landfast sea ice approximately 1 km off the coast of Barrow, Alaska at 71° 21' 56.45" N, 156° 32' 39.01" W. The measurements were made during the northern hemisphere spring at roughly one to two weekly intervals over the period April-June 2008. A sea ice mass balance site was operated by the University of Alaska Fairbanks at the same location recording snow and ice thickness, sea level, relative humidity and air, ice and water temperatures (Druckenmiller et al., 2009). The electrode strings used in the resistivity measurements were as described by Ingham et al. (2008) and were deployed at the corners of a 1 m x 1 m square, allowing measurements to be made through the undisturbed sea ice between boreholes.

519

520 On each of the 6 occasions measurements of the horizontal resistivity were made between
521 each of the six borehole pairs, with each measurement involving one current and one
522 potential electrode in each borehole, according to the criteria discussed above. Thus, it is
523 assumed that the measurements allow an accurate estimate of ρ_H , in the volume contained by
524 the boreholes, to be derived by 3D inversion. Similarly, a combination of measurements
525 aimed at determining ρ_m were obtained using a four electrode array with each of the
526 electrodes at approximately the same depth in separate boreholes, and three electrodes at the
527 same depth in separate boreholes and a remote surface electrode. As discussed previously it is
528 assumed that inversion of this data set yields an estimate ρ_m^M of the geometric mean
529 resistivity which is an underestimate of the true value ρ_m .

530

531 The datasets for determination of ρ_H contained approximately 2500 separate measurements.
532 Those for ρ_m were smaller and contained between 350 and 400 separate measurements. The
533 ice thickness at the time of each set of measurements was determined from ice temperature
534 measurements and cores. In inversions of the data the thickness values were used to set the
535 initial resistivity below the ice to approximate the resistivity of the underlying seawater (0.4
536 Ωm). This value was made "sticky" so as to control its degree of change during the
537 inversions. The 3D inversions for ρ_H typically took 4-6 iterations and gave final rms misfits
538 of between 10 and 16%, while those for ρ_m took 5-6 iterations and gave final misfits of 2-
539 10%. Much of the misfit in the ρ_H inversions occurs in the region of the ice-water interface.
540 In this region the transition from high resistivity within the ice to the low resistivity sea water
541 is clearly more complex than for the theoretical models discussed above. As a result it
542 appears that electrodes spaced at vertical intervals of 0.1 m are not able to sample finely

543 enough to accurately resolve the rapid change in resistivity from several hundred Ωm to a
544 value less than 1 Ωm over a vertical distance of typically a few centimeters. The (assumed)
545 much smaller decrease in ρ_m across this same region can, in contrast, be much better
546 reproduced.

547
548 Sections through the resulting resistivity structures, obtained from the 3D inversions of data
549 measured on the 8-9 May 2008, showing ρ_H and ρ_m^M are shown in Fig. 5 (a) and (b)
550 respectively. The inversions use a grid with horizontal spacing of 0.05 m in both x and y
551 directions, and a vertical spacing of 0.1 m. Above the immediate vicinity of the ice-water
552 interface, at approximately 1.35 m depth (from ice thickness measurements), ρ_H is seen to be
553 essentially uniform throughout the body of the ice and to have a value around 600 Ωm . Some
554 variation appears in the derived value of ρ_m^M but in general, above the ice-water interface it
555 lies in the range 10-20 Ωm . The vertical discretisation of the model leads to sharp gradients
556 in the recovered values of resistivity between depths of 1.3 and 1.4 m.

557
558 As discussed above, synthetic data sets generated for different values of the anisotropy
559 coefficient allow parameterization of the degree to which, for the observed ice thickness, ρ_m^M
560 is an underestimate of the true value of the geometric mean resistivity ρ_m . Synthetic data
561 generated for different values of anisotropy λ for the measured ice thickness, 1.35 m on 8-9
562 May 2008, have been used to derive the appropriate polynomial $F_z(\lambda)$ for each depth range in
563 the 3D models. The polynomials have then been used, with the average values of ρ_H and ρ_m^M
564 for each layer in the resistivity models shown in Fig. 5, to estimate the actual variation of λ
565 with depth in the ice through numerical solution of (21). These values have then been used
566 with the values of ρ_H to determine not only the true values of ρ_m through the ice, but also to

derive the vertical component of the bulk resistivity ρ_V . The standard deviations associated with the average values of ρ_H and ρ_m^M in each layer allow at least a superficial estimate of the uncertainties in λ , ρ_m and ρ_V . The results of this analysis are shown in Fig. 6 which shows the derived variation with depth of all three resistivities and the anisotropy coefficient.

For the 8-9 May measurements the anisotropy coefficient is found to be close to 0.24 through the entire thickness of the ice down to 1.3 m depth. Although the higher values calculated between 1.3 and 1.4 m are not unreasonable given the expected increase in connectivity of brine at the base of the ice, it must be remembered that this depth range spans the actual ice-water interface and the values of ρ_H and ρ_m^M in this region are not well resolved even though standard deviations calculated from the 3D models are relatively small. The derived values of λ are slightly less than values found, for example, by Timco (1979) at Pond Inlet, N.W.T. (0.59) and Buckley et al. (1986) in the Antarctic (~0.5), but are not unreasonable for sea ice formed under the quiescent conditions which tend to exist at Barrow. The corrected values for ρ_m (~ 150 Ωm) are well within the ranges previously measured by other authors using surface resistivity soundings. However, a Wenner array surface sounding taken adjacent to the location of the boreholes on 9 May 2008 yielded apparent resistivity values at small electrode spacing ($a = 0.1 - 0.4$ m) of 40-50 Ωm , a factor of about 3 smaller than the values shown in Fig. 6. This lends some support to the suggestion that, notwithstanding the small standard deviations in the resolved resistivity values, the cumulative effect of uncertainties and approximations in the derivation of ρ_m may mean that the derived values should be regarded as an estimate correct to within a factor of 3-4. However, various authors have previously noted the non-uniqueness in the interpretation of Wenner soundings, particularly the distortions in derived depth variations that occur in interpretation due to the anisotropic

nature of the resistivity. It could therefore be argued that the estimates of ρ_m derived from the cross-borehole results are in fact more reliable. In the context of mapping how the resistivity structure of sea ice varies with time over a series of measurement sequences such an unresolved ambiguity may not necessarily be crucial.

Each of the datasets in the entire sequence of measurements from April-June 2008 was treated in the manner described above to derive both the horizontal and vertical components of resistivity. Vertical sections through the derived models for ρ_H and the calculated profiles for ρ_V , for all six sets of measurements are shown in Fig. 7. From these results it is clear that, as originally found by Ingham et al. (2008) for ρ_H , there are significant temporal changes in resistivity as spring warming occurs. These may be summarized as follows:

(1) there is a gradual decrease of ρ_H from over 1000 Ωm to about 350 Ωm between early April and the end of May.

(2) A similar, but smaller, change in the vertical component of resistivity ρ_V occurs over the same period. Values decrease from 40-70 Ωm in early April to less than 30 Ωm by the end of May.

(3) Despite these changes the anisotropy coefficient λ remains approximately constant with values (0.2 - 0.3) similar to those shown in Fig. 6.

(4) A more significant change in the horizontal component of resistivity take place between the end of May and mid-June during which the resistivity decreases by a factor of about 6. During this period there was a considerable thinning of the ice as well as surface ablation which left the upper 3 electrodes in each string no longer embedded in the ice.

(5) Over this period in early June there was also a decrease in the vertical resistivity between 0.5 and 1 m depth, while at shallower depths the infiltration of fresh water, from melt ponds formed on the surface, led to an increase in ρ_V .

616

617 **5. Discussion**

618

619 Many authors have discussed pronounced changes in the physical properties of sea ice with
620 time and temperature. For example Buckley and Trodahl (1987) commented on changes in
621 the optical behaviour of Antarctic sea ice related to a 10 °C increase in temperature. Pringle et
622 al. (2007), in studying the thermal conductivity of sea ice, estimated that periodic internal
623 motion of brine within the ice due to convection could contribute to the total heat flow
624 through the ice. Golden et al. (2006) have also emphasised the importance of the fluid
625 permeability of sea ice for not only understanding brine drainage and the growth of ice, but
626 also the transport of nutrients and pollutants through sea ice. In particular, below -5 °C sea ice
627 appears to be vertically impermeable (Weeks and Ackley, 1986), whereas above this
628 temperature it is permeable (Golden et al., 2007).

629

630 The results shown in Fig. 7 are possibly the first presentation of the temporal evolution of an
631 anisotropic physical property of sea ice. They make it clear that the electrical properties of
632 sea ice undergo significant changes. Detailed modelling of ice structure to attempt to fully
633 understand how these changes relate to temperature, salinity and brine volume fraction (ϕ_b)
634 remains to be carried out. Nevertheless it is likely, as is discussed further below, that the
635 decrease in both principal components of resistivity between early April and late May is
636 related to an increase in ϕ_b as the ice warms. However, the relatively low values of vertical
637 resistivity which exist even when the ice is still cold in early April, suggests that, although the
638 ice may be impermeable to fluid transport, a certain degree of electrical connectivity exists at
639 all times. Given the apparent existence of vertical electrical connection, the implications for

fluid permeability of the structural changes which lead to the changes in electrical resistivity warrant considerable attention.

Some initial indication of the nature of the variation of resistivity with brine volume fraction can be gained by calculating the manner in which the formation factor, FF , (defined as the ratio of the bulk resistivity ρ of a saturated medium to the resistivity of its pore fluid, ρ_b) varies with ϕ_b . The concept of formation factor derives from Archie's Law (Archie, 1942) which relates these parameters through the expression

$$FF = \frac{\rho}{\rho_b} = C \phi_b^{-m} \quad (23)$$

in which C and m are empirically determined constants. The first of these constants, C , is a function of the microstructure of the medium and, as long as the geometry of this remains unchanged a log-log plot of formation factor against brine volume fraction yields a straight line of slope $-m$. For the resistivity models shown in Fig. 7, the corresponding values of brine resistivity can be calculated from the measured temperature data using the relationship of Morey et al. (1984), and brine volume fractions can be found from measured temperature and salinity data using the expressions of Cox & Weeks (1983). The resulting log-log plots of FF against ϕ_b for both the horizontal and vertical components of the bulk resistivity are shown in Fig. 8 and, for brine volume fractions less than 10%, clearly confirm the expected linear variation. In addition to this, however, the sharp drop in the horizontal component of resistivity between late May and mid-June, which is prominent in Fig. 7, appears as a sharp discontinuity in the formation factor plot. This is possibly indicative of a fundamental change in the microstructure of the ice and suggests that a percolation threshold such as proposed by Golden et al. (1998, 2007) may have been crossed. Ingham et al. (2008) tentatively suggested that such a threshold might occur for the horizontal component of resistivity at a brine

volume fraction of about 8%. That estimate was based, however, on three sets of much sparser data acquired using only 2 boreholes. Detailed analysis and structural modelling of the present results should give a much clearer indication of any such threshold and also provide information on the existence of any percolation transition for the vertical component of resistivity.

The vertical conductivity structure, in particular the near-constant values of the anisotropy coefficient λ shown in Fig. 6, also suggests that vertical microstructural variations associated with the transition from granular to columnar ice (which was observed to occur at depths between 20 and 40 cm in the vicinity of the measurement site) are not strongly reflected in the resistivity structure. While this finding requires more detailed analysis and measurements at finer vertical resolution, it may suggest that in granular ice, rather than the isotropic primary pore space, it is the anisotropic secondary pores (such as brine tubes and channels) that control the resistivity structure. Similarly, the impact of vertical variations in brine volume fractions is only marginally expressed in the structure of ρ_H and ρ_V (Fig. 6).

6. Summary

We have shown theoretically that suitable combinations of cross-borehole dc resistivity measurements may be used to measure directly the value of the horizontal component of the resistivity in sea ice or other anisotropic medium within which $\rho_V < \rho_H$. Furthermore, although the particular structure of sea ice means that exact measurement of the geometric mean resistivity is not possible, we have demonstrated that it is also possible to make measurements which, in association with numerical modelling, allow a reasonable estimate of ρ_m to be derived. As a consequence estimates of the vertical component of resistivity, which

cannot be directly measured, can also be obtained. The technique is illustrated by the results of a series of measurements made on first-year sea ice at Barrow, Alaska. These clearly show that the electrical resistivity of sea ice varies significantly with time and temperature. The development described here thus opens the way for understanding the microstructural changes that occur within sea ice and the implications of these for the behaviour of other transport properties. It therefore has the potential to contribute significantly to the understanding of sea ice microstructure and its response to changes in temperature, salinity and ϕ_b .

Acknowledgements

KJ is supported by a Victoria University of Wellington Postgraduate Assistantship. We acknowledge financial support through NSF Office of Polar Programs Grants ARC-0620124 and 0934683, and logistic support provided by the Barrow Arctic Science Consortium. The authors wish to thank Hugh Bibby and two anonymous reviewers for comments on an earlier version of the manuscript.

708 **References**

709

710 Archie, G.E. (1942), The electrical resistivity log as an aid in determining some reservoir
711 characteristics, *Trans. Am. Inst. Min. Metall. Eng.*, 146, 54-62.

712

713 Bhattacharya, P.K. and H.P. Patra (1968), *Direct current geoelectric sounding: Principles*
714 *and interpretation*, 139 pp., Elsevier Publishing, Amsterdam.

715

716 Buckley, R.G., M.P. Staines and W.H. Robinson (1986), In situ measurements of the
717 resistivity of Antarctic sea ice, *Cold Reg. Sci. Technol.*, 12, 285-290.

718

719 Buckley, R.G. and H.J. Trodahl (1987), Thermally driven changes in the optical properties of
720 sea ice, *Cold Reg. Sci. Technol.*, 14, 201-204.

721

722 Callaghan, P.T., C.D. Eccles, T.G. Haskell, P.J. Langhorne and J.D. Seymour (1998), Earth's
723 field NMR in Antarctica: a pulsed gradient spin echo NMR study of restricted diffusion in
724 sea ice, *J. Magn. Reson.*, 133, 148–154.

725

726 Callaghan, P.T., R. Dykstra, C.D. Eccles, T.G. Haskell and J.D. Seymour (1999), A nuclear
727 magnetic resonance study of Antarctic sea ice brine diffusivity, *Cold Reg. Sci. Technol.*, 29,
728 153–171.

729

730 Cherkaeva, E. and K.M. Golden (1998), Inverse bounds for microstructural parameters of
731 composite media derived from complex permittivity measurements, *Waves in Random*
732 *Media*, 8, 437-450.

733

734 Comiso, J. C. (2003), Large scale characteristics and variability of the global sea ice cover, in

735 *Sea Ice: An introduction to its Physics, Chemistry, Biology and Geology*, edited by D.N.

736 Thomas and G.S. Dieckmann, pp. 112-142, Blackwell Science Ltd, Oxford.

737

738 Cox, G. F. N. and W. F. Weeks (1983), Equations for determining the gas and brine volumes

739 in sea-ice samples, *J. Glaciol.*, 29, 306-316.

740

741 de Groot-Hedlin, C. and S. Constable (1990), Occam's inversion to generate smooth two-

742 dimensional models from magnetotelluric data, *Geophysics*, 55, 1613-1624.

743

744 Dieckmann, G.S. and H.H. Hellmer (2003), The importance of sea ice: An overview, in *Sea*

745 *Ice: An introduction to its Physics, Chemistry, Biology and Geology*, edited by D.N. Thomas

746 and G.S. Dieckmann, pp. 1-21, Blackwell Science Ltd, Oxford.

747

748 Druckenmiller, M.L., H. Eicken, M.A. Johnson, D.J. Pringle, and C.C. Williams (2009),

749 Towards an integrated coastal sea-ice observatory: System components and a case study at

750 Barrow, Alaska, *Cold Reg. Sci. Technol.*, 56, 61-72

751

752 Eicken, H. (2003). From the microscopic, to the macroscopic, to the regional scale: Growth,

753 microstructure and properties of sea ice, in *Sea Ice: An introduction to its Physics, Chemistry,*

754 *Biology and Geology*, edited by D.N. Thomas and G.S. Dieckmann, pp. 22-81, Blackwell

755 Science Ltd, Oxford.

756

757 Eicken, H., C. Bock, R. Wittig, H. Miller and H.-O. Poertner (2000), Magnetic resonance
758 imaging of sea ice pore fluids: methods and thermal evolution of pore microstructure, *Cold*
759 *Reg. Sci. Technol.*, *31*, 207–225.

760

761 Freitag, J. and H. Eicken (2003), Melt water circulation and permeability of Arctic summer
762 sea ice derived from hydrological field experiments, *J. Glaciol.*, *49*, 349–358.

763

764 Fritsen, C.H., V.I. Lytle, S.F. Ackley, S.F. and C.W. Sullivan (1994), Autumn bloom of
765 Antarctic pack-ice algae, *Science*, *266*, 782-784.

766

767 Fujino, K. and Y. Suzuki (1963), An attempt to estimate the thickness of sea ice by electrical
768 resistivity method II, *Low Temp. Sci.*, *A21*, 151–157.

769

770 Golden, K.M., S.F. Ackley and V.I. Lytle (1998), The percolation phase transition in sea ice.
771 *Science*, *282*, 2238-2241.

772

773 Golden, K.M., A.L. Heaton, H. Eicken and V.I. Lytle (2006), Void bounds for fluid transport
774 in sea ice, *Mechanics of Materials*, *38*, 801-817.

775

776 Golden, K. M., H. Eicken, A.L. Heaton, J. Miner, D.J. Pringle and J. Zhu (2007), Thermal
777 evolution of permeability and microstructure in sea ice, *Geophys. Res. Lett.*, *34*, L16501,
778 doi:10.1029/2007GL030447

779

780 Hallikainen, M. and D.P. Winebrenner (1992), The physical basis for sea ice remote sensing,
781 in *Microwave Remote Sensing of Sea Ice*, edited by F.D. Carsey, pp. 29-46, Geophysical
782 Monograph, vol. 68, American Geophysical Union, Washington.

783

784 Hashin, Z. and S. Shtrikman (1962), A variational approach to the theory of the effective
785 magnetic permeability of multiphase materials, *J. Appl. Phys.*, 33, 3125-3131.

786

787 Ingham, M., D. Pringle, and H. Eicken (2008), Cross-borehole resistivity tomography of sea
788 ice, *Cold Reg. Sci. Technol.*, 52, 263-277.

789

790 Kawamura, T. (1988), Observations of the internal structure of sea ice by x ray computed
791 tomography, *J. Geophys. Res.*, 93, 2343-2350.

792

793 Keller, G. V. and F.C. Frischknecht (1966), *International series of monographs in*
794 *electromagnetic waves Volume 10: Electrical methods in geophysical prospecting*, Pergamon
795 Press, Oxford.

796

797 Kovacs, A. and R., Morey (1978), Radar anisotropy of sea ice due to preferred azimuthal
798 orientation of the horizontal c axes of ice crystals, *J. Geophys. Res.*, 83(C12), 6037-6046.

799

800 Krembs, C., R. Gradinger, and M. Spindler (2000), Implications of brine channel geometry
801 and surface area for the interaction of sympagic organisms in Arctic Sea ice, *J. Exp. Mar.*
802 *Biol. Ecol.*, 243, 55–80.

803

804 Loke, M.H. and R.D. Barker (1996), Rapid least-squares inversion of apparent resistivity
805 pseudosections by a quasi-Newton method, *Geophysical Prospecting*, 44, 131-152.
806

807 Loke, M.H. and T. Dahlin (2002), A comparison of the Gauss-Newton and quasi-Newton
808 methods in resistivity imaging inversions, *Journal of Applied Geophysics*, 49, 149-162.
809

810 Mercier, O.R., M.W. Hunter, and P.T. Callaghan (2005), Brine diffusion in first-year sea ice
811 measured by Earth's field PGSE-NMR, *Cold Reg. Sci. Technol.*, 42, 96–105.
812

813 Morey, R. M., A., Kovacs, and G. F. N., Cox (1984), Electromagnetic properties of sea ice,
814 *Cold Reg. Sci. Technol.*, 9, 53-75.
815

816 Notz, D. and M. G. Worster (2008), In situ measurements of the evolution of young sea ice,
817 *Journal of Geophysical Research*, 113, C03001, doi:10.1029/2007JC004333
818

819 Perovich, D.K. (1998), Optical properties of sea ice, in: *Physics of Ice-Covered seas*, editor
820 M. Lepparanta, pp. 195-230, Springer-Verlag, New York.
821

822 Pringle, D.J., H. Eicken, H.J. Trodahl, and L.G.E. Backstrom (2007), Thermal conductivity
823 of landfast Antarctic and Arctic sea ice, *J. Geophys. Res.*, 112, C04017,
824 doi:10.1029/2006JC003641.
825

826 Pringle, D., G. Dubuis, and H. Eicken (2009a), Impedance measurements of the complex
827 dielectric permittivity of sea ice at 50 MHz: pore microstructure and potential for salinity
828 monitoring, *J. Glaciol.*, 55, 81-94.

829

830 Pringle, D. J., J.E. Miner, H. Eicken and K.M. Golden (2009b). Pore-space percolation in sea
831 ice single crystals. , *J. Geophys. Res.*, *114*, C12017, doi:10.1029/2008JC005145.

832

833 Sasaki, Y. (1992), Resolution of resistivity tomography inferred from numerical simulation,
834 *Geophysical Prospecting*, *40*, 453-464.

835

836 Telford, W. M., L.P. Geldart, R.E. Sheriff and D.A. Keys (1977), *Applied Geophysics*,
837 Cambridge University Press, New York.

838

839 Thyssen, F., H. Kohnen, M.V. Cowan and G.W. Timco (1974), DC Resistivity measurements
840 on sea ice near Pond Inlet, N.W.T (Baffin Island), *Polarforschung*, *44*, 117-126.

841

842 Timco, G.W. (1979), An analysis of the in-situ resistivity of sea ice in terms of its
843 microstructure, *J. Glaciol.*, *22*, 461–471.

844

845 Tinga, W.R., W.A.G. Voss, and D.F. Blossey, (1973), Generalized approach to multiphase
846 dielectric mixture theory, *J. Appl. Phys.*, *44*, 3897-3902.

847

848 Weeks, W.F. (1998), Growth conditions and the structure and properties of sea ice in: *Physics*
849 *of Ice-Covered seas*, editor M. Lepparanta, pp. 25-104, Springer-Verlag, New York.

850

851 Weeks, W.F. and S.F. Ackley (1986), The growth, structure and properties of sea ice, in *The*
852 *Geophysics of Sea Ice*, edited by N. Untersteiner, pp. 9-164, Plenum Press, New York.

853

854

855

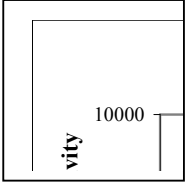
Figure captions.

Fig. 1 Geometry for the calculation of the potential at electrode P , at (x_j, y_j, z_j) , due to current injected at electrode C , at (x_i, y_i, z_i) , for the case of a semi-infinite anisotropic medium in the region $z > 0$. The horizontal separation of the electrodes is $X_{ij} = \sqrt{(x_i - x_j)^2 + (y_i - y_j)^2}$.

Fig. 2 Variation of horizontal resistivity ρ_H with depth recovered by 3D inversion of synthetic borehole measurements for the case of sea ice of thickness $t = 1.4$ m, anisotropy coefficient $\lambda = 0.1$, and geometric mean resistivity $\rho_m = 100 \Omega\text{m}$. The true value of ρ_H is shown by the dashed line.

Fig. 3 Variation with depth of the value of geometric mean resistivity ρ_m^M recovered by 3D inversion of synthetic data sets with different values of anisotropy coefficient λ for a true value of the geometric mean resistivity of $100 \Omega\text{m}$ and a model ice thickness of 1.4 m shown by the solid line..

Fig. 4 Hashin-Shtrickman bounds on the resistivity of a 2-phase mixture in which one component has a resistivity of $0.4 \Omega\text{m}$ and the other a resistivity of $600 \Omega\text{m}$. The upper (dashed) curve shows the bulk resistivity as a function of volume fraction of the high conductivity component when that component occurs as isolated spheres, the lower (solid) curve shows the bulk resistivity when the high conductivity component forms a the connected network in which the spheres are embedded.



879 Fig. 5 Vertical sections through 3D structures of (a) ρ_H and (b) ρ_m^M derived by 3D inversion
 880 of field data collected at Barrow over May 8-9 2008. Horizontal distances and depths are both
 881 in m.

882

883 Fig. 6 Variations with depth of ρ_H , ρ_m , ρ_V and λ derived from field data collected at Barrow
 884 over May 8-9 2008. Thin lines show limits of the derived values calculated from standard
 885 deviations in the average values of ρ_H and ρ_m^M .

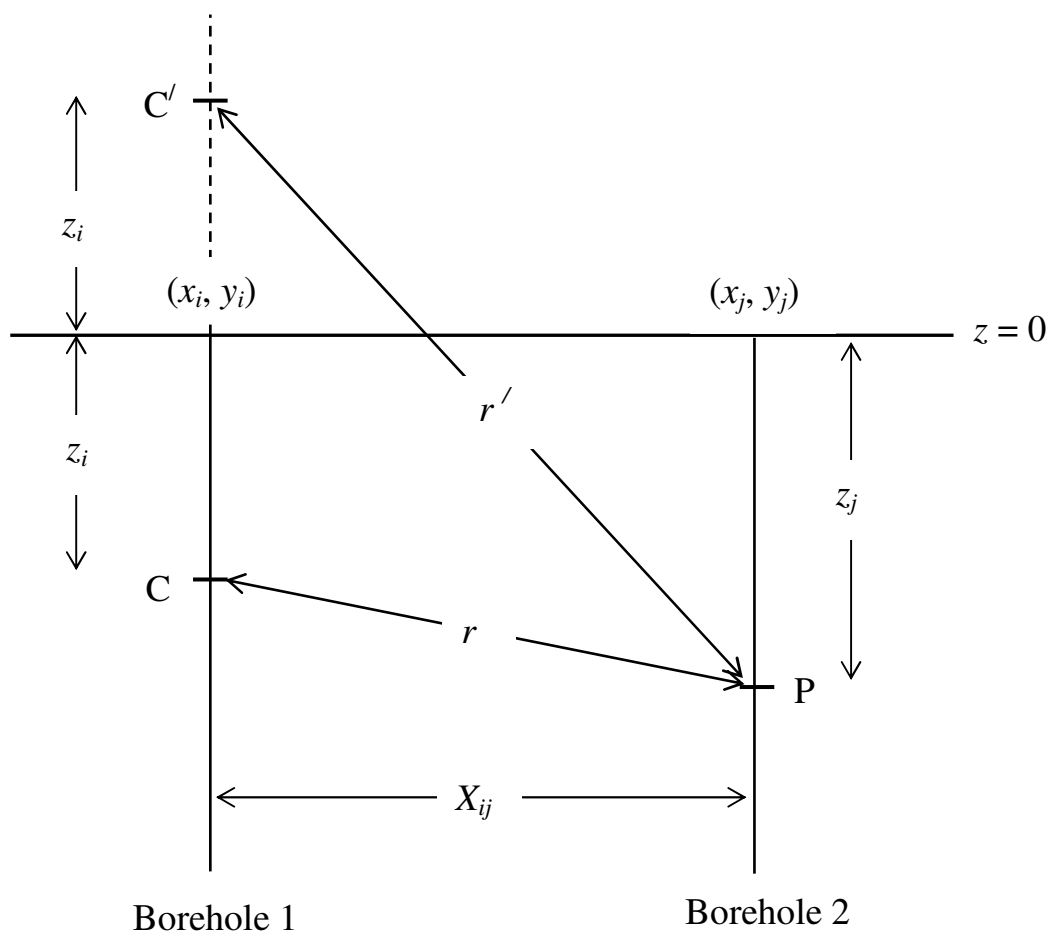
886

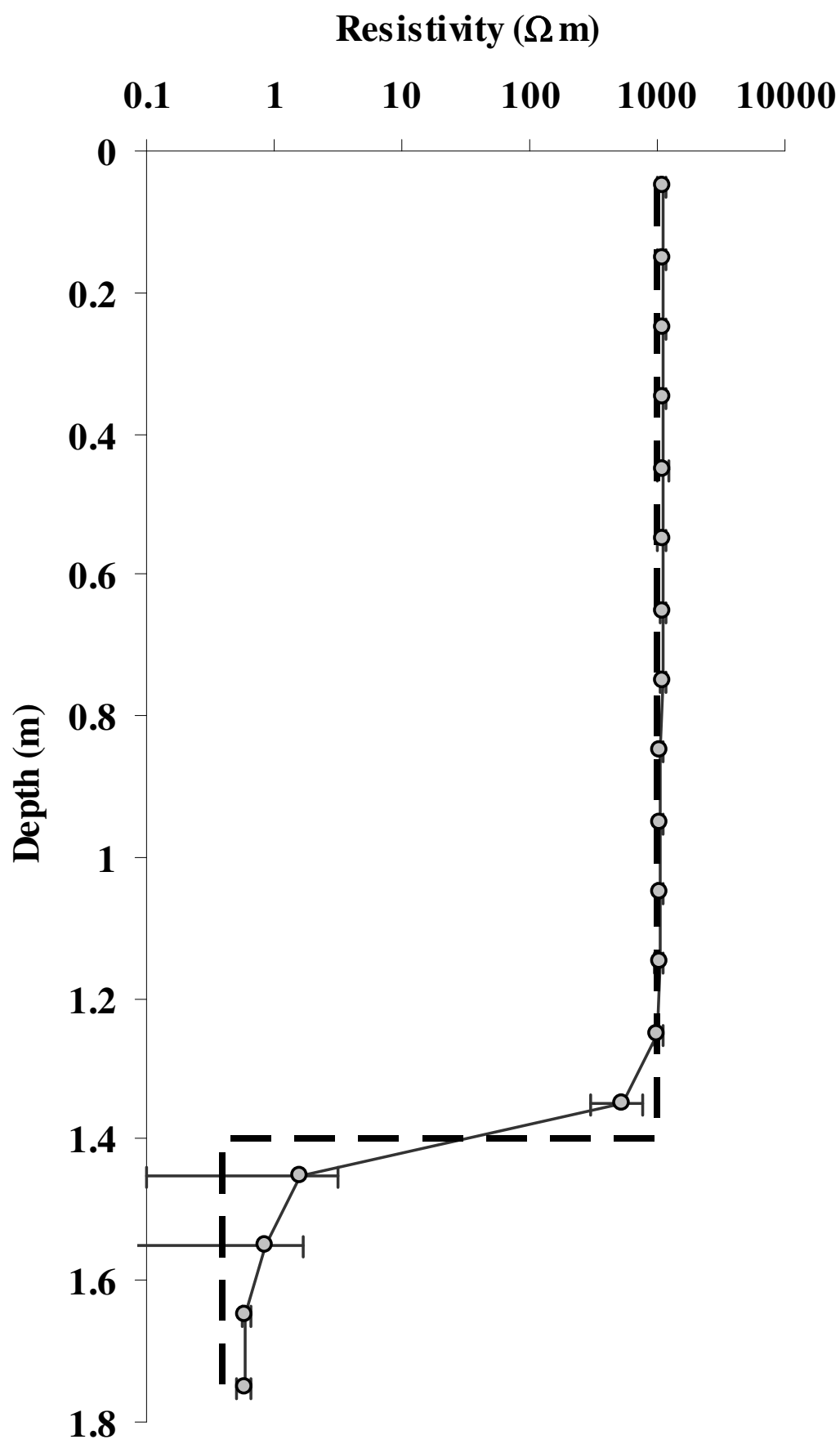
887 Fig. 7 Vertical sections through derived ρ_H and calculated ρ_V structures for a sequence of 6
 888 dates between April and June 2008. The top row shows ρ_H , the bottom row ρ_V . Horizontal
 889 distances and depths are both in m.

890

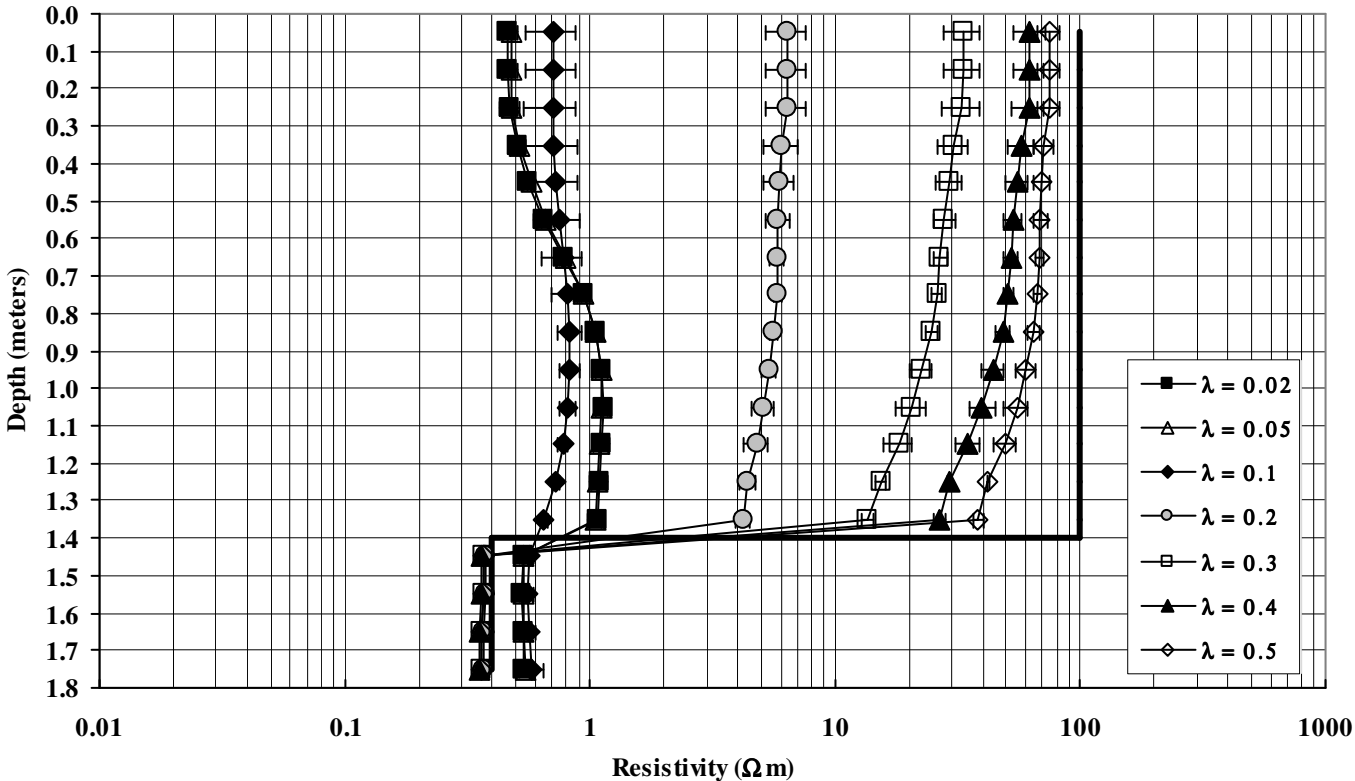
891 Fig. 8 Plots of formation factor (ρ/ρ_b) against brine volume fraction (ϕ_b) for horizontal and
 892 vertical components of resistivity. Filled circles are data from 7-9 April, filled squares from
 893 25-26 April, filled diamonds from 8-9 May, filled triangles from 20-21 May, open circles
 894 from 28-29 May, and open squares from 16-17 June.

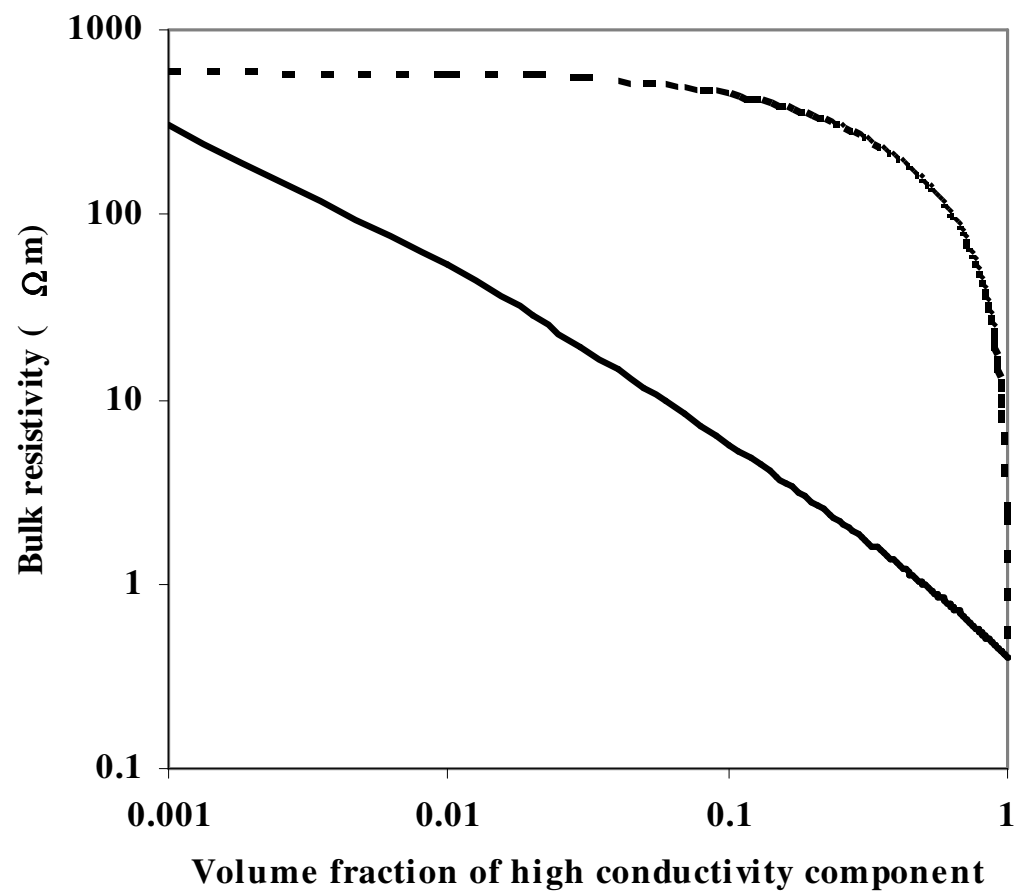
895

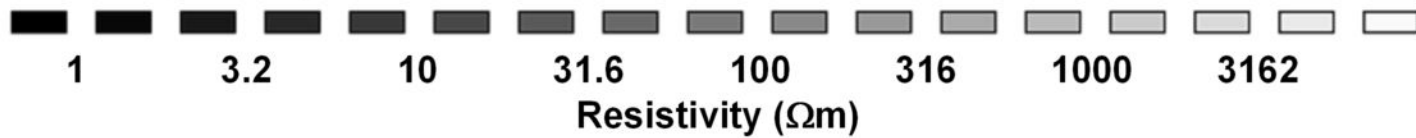
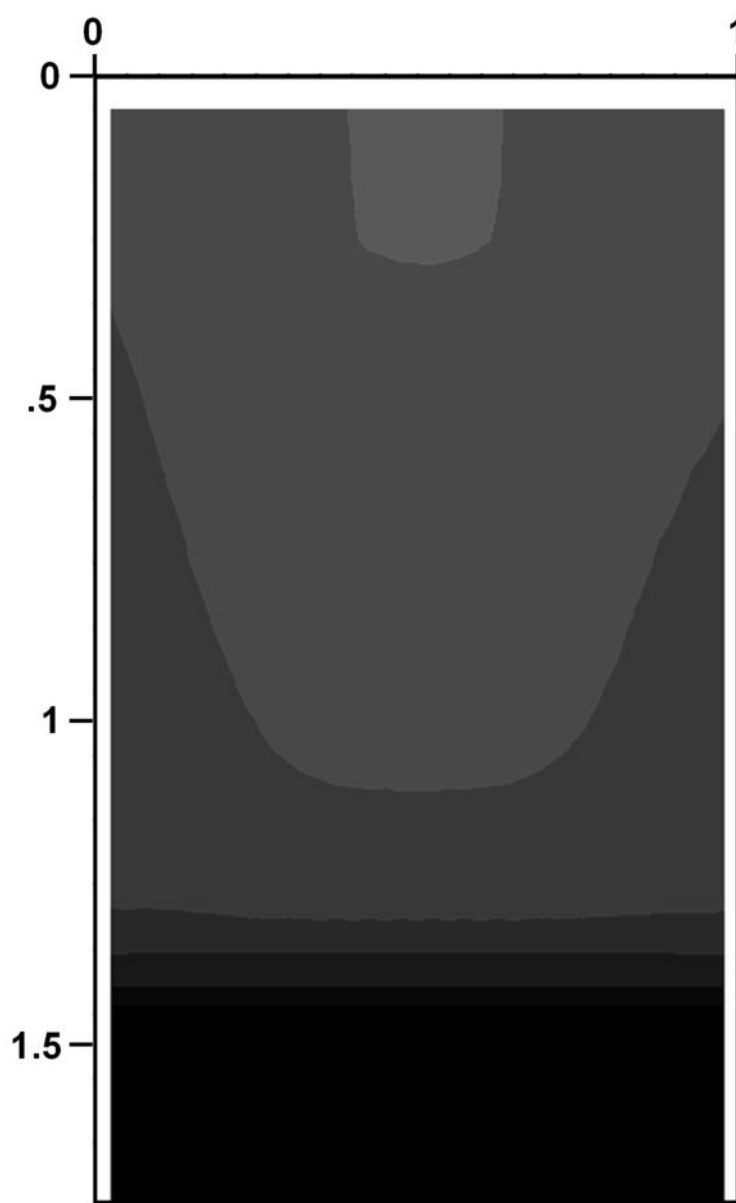
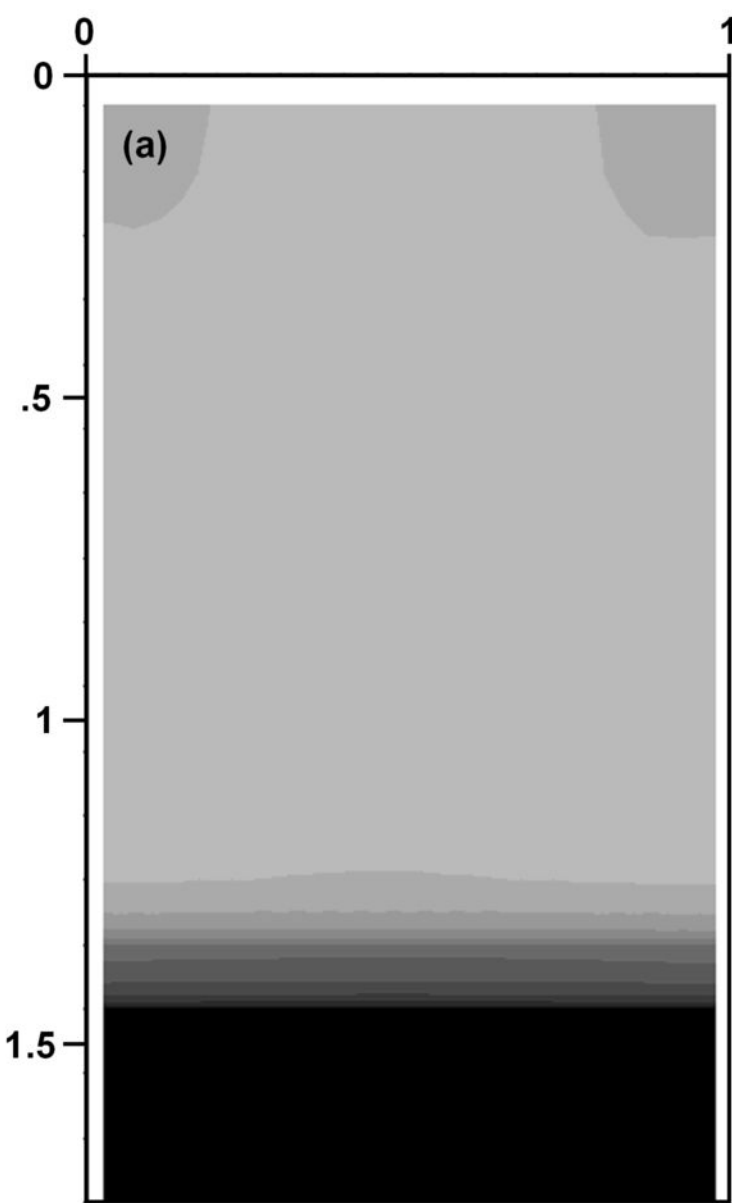


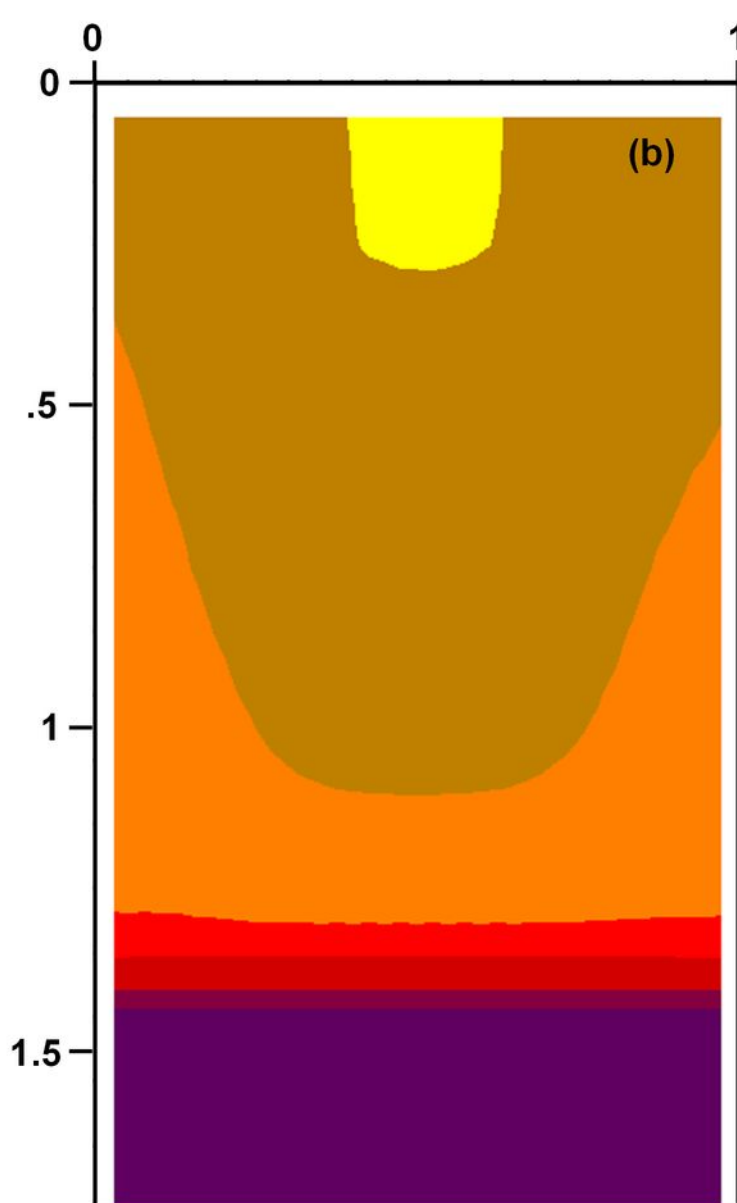
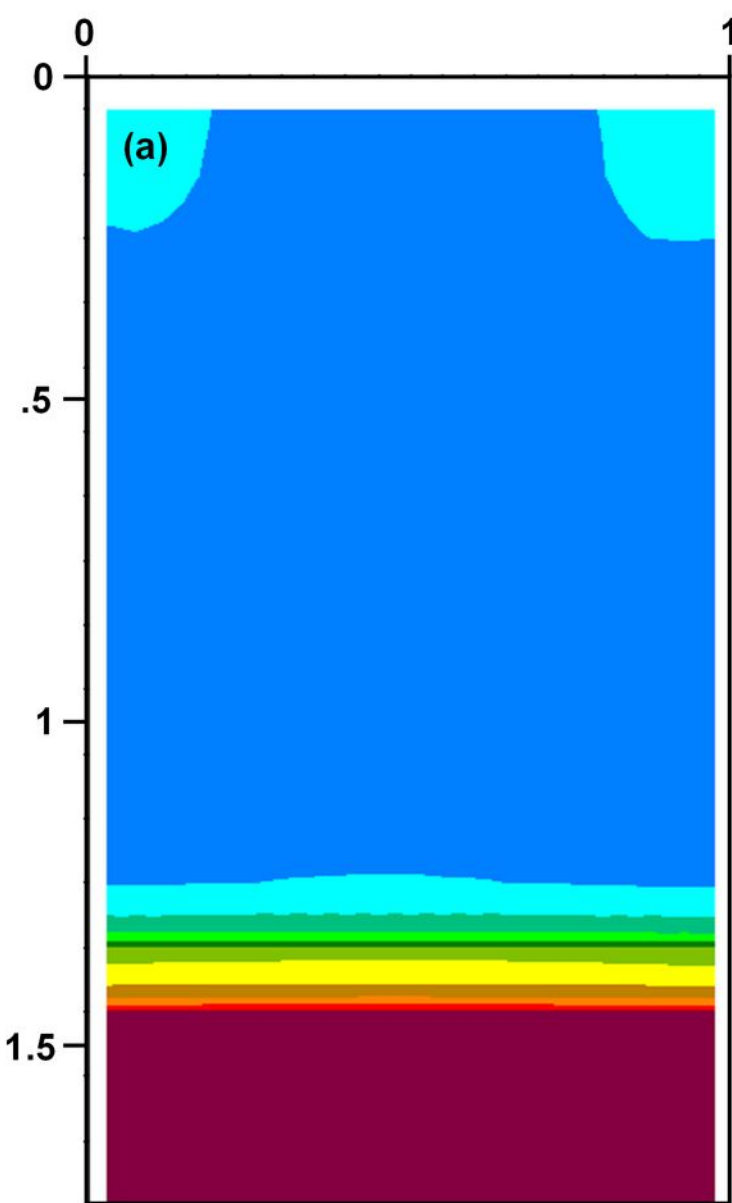


Average recovered geometric mean resistivity as a function of depth for t = 1.4 m

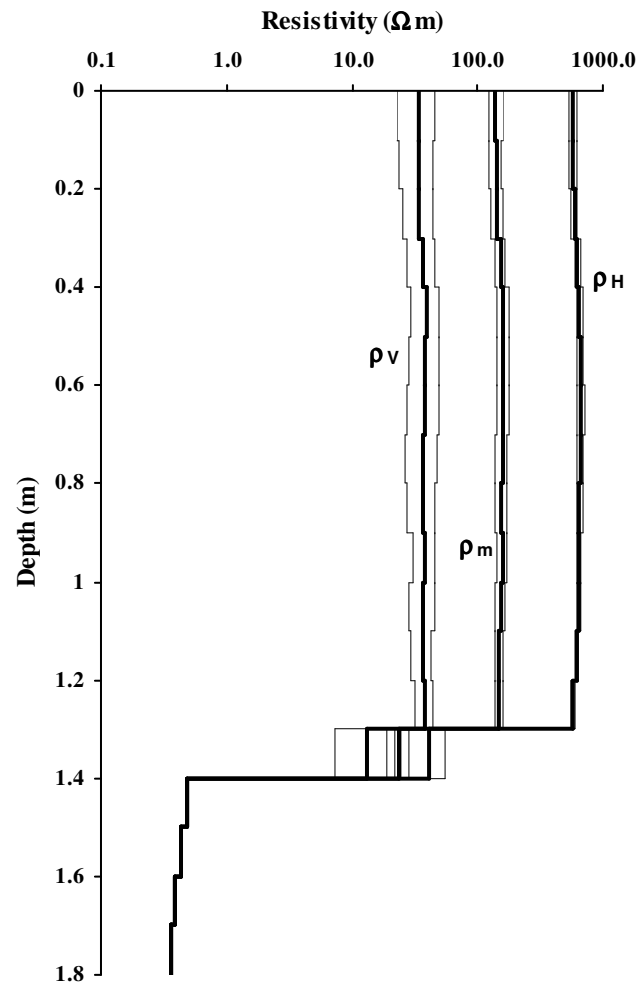




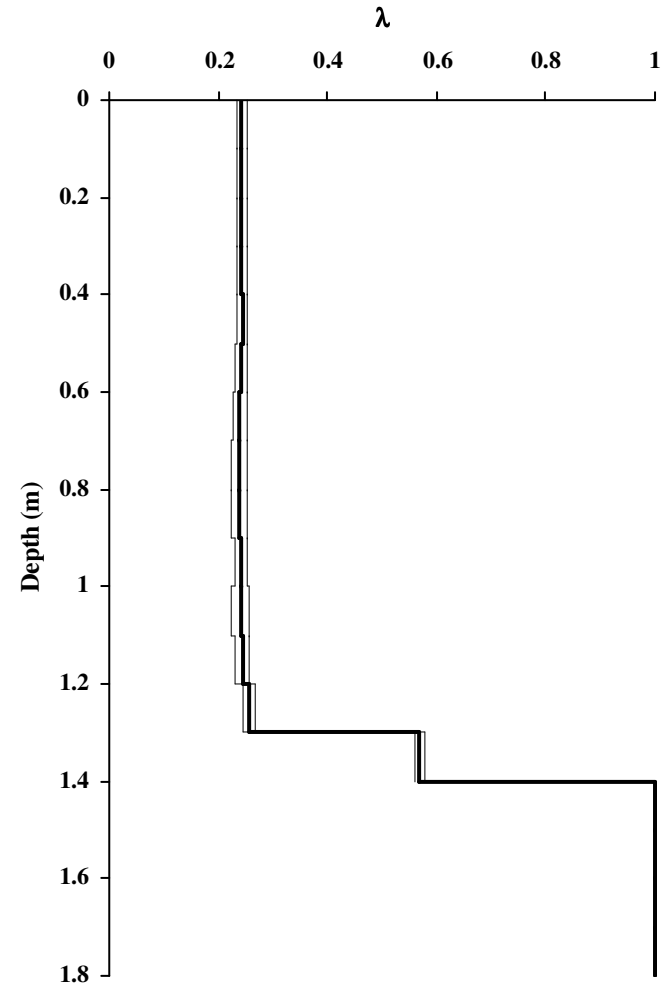


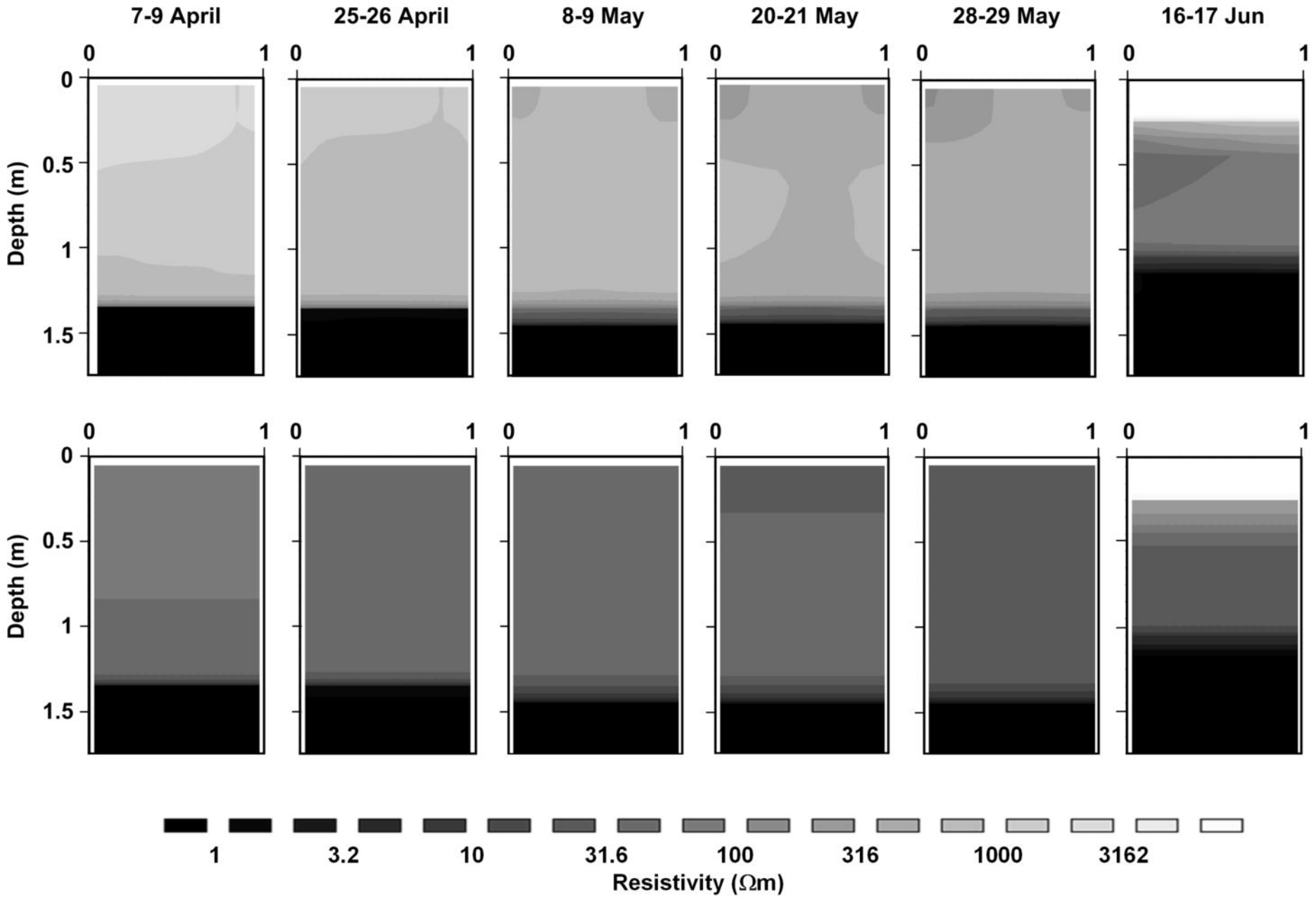


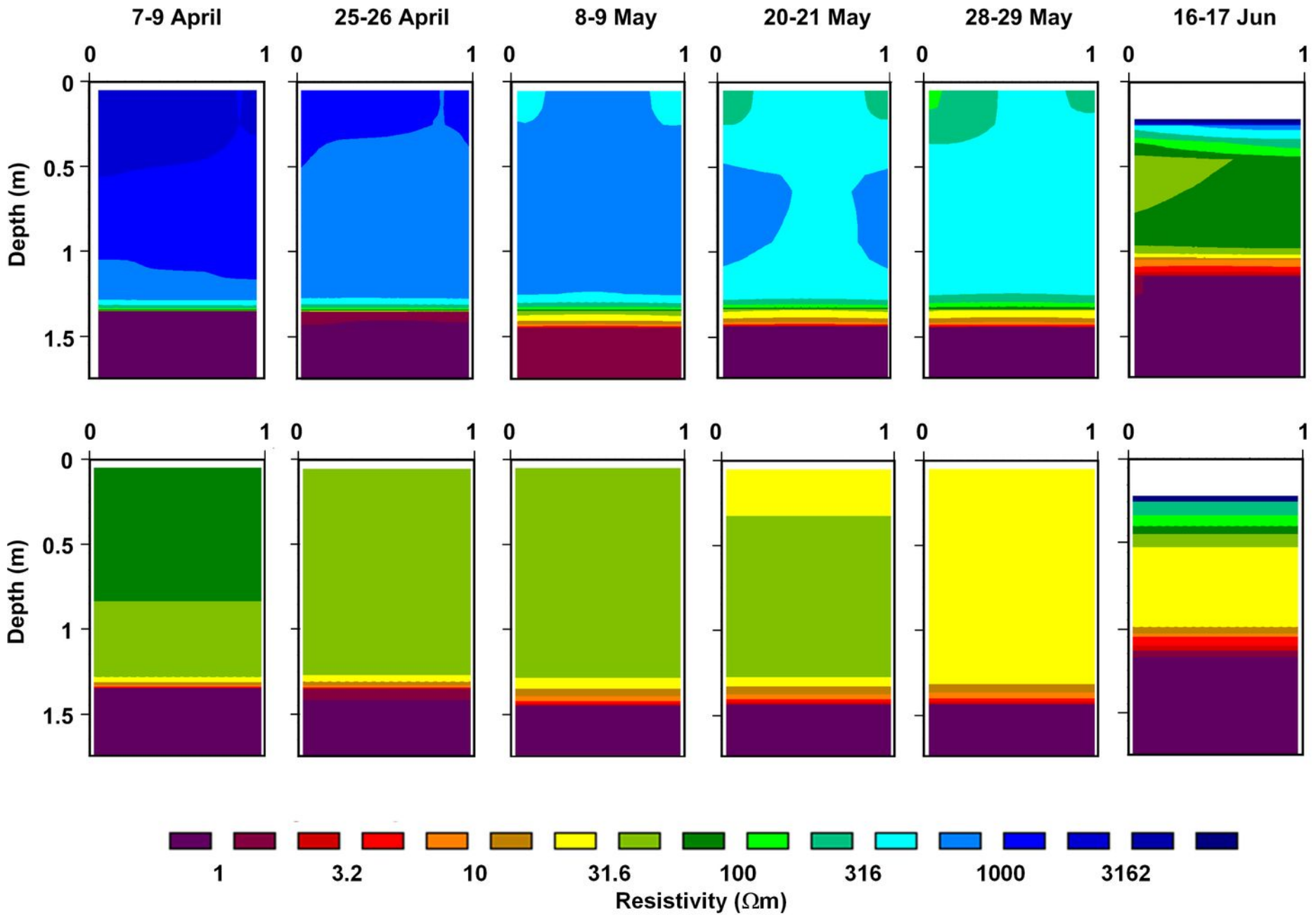
Resistivity v Depth May 08/09 2008



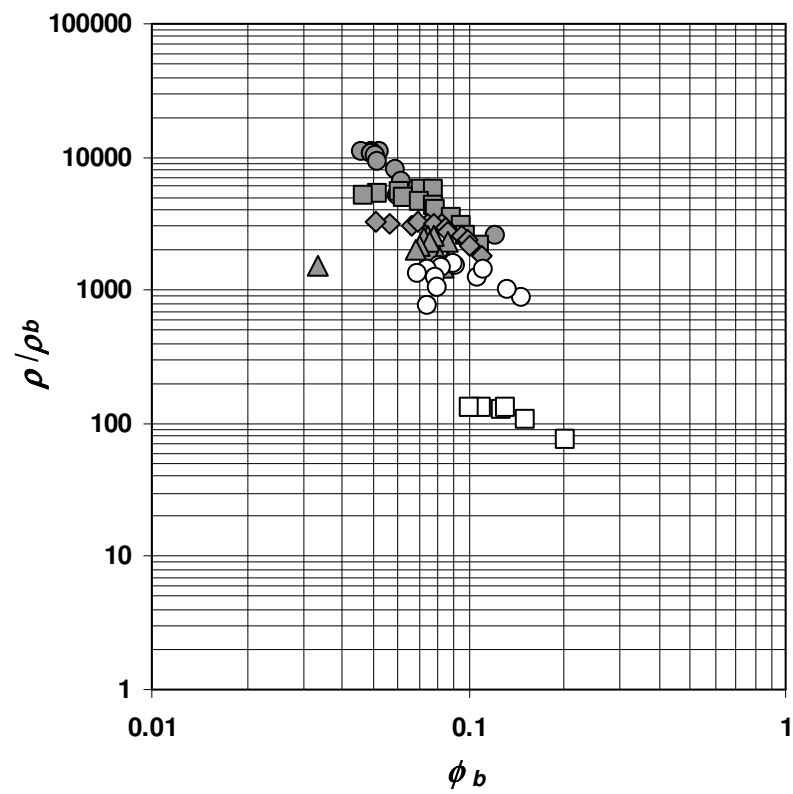
λ v Depth







Horizontal formation factor



Vertical formation factor

